A simple method for Bragg diffraction in volume holographic gratings

Alexander Heifetz,[a] John T. Shen, and M. S. Shahriar
Department of Electrical Engineering and Computer Science, Northwestern University, Evanston, Illinois 60208

(Received 19 February 2007; accepted 21 April 2009)

We discuss a simple beam interference approximation method for deriving the angular selectivity of diffraction in weakly modulated volume holographic gratings. The results obtained using the multiple beam interference model agree qualitatively with the results obtained from a physical optics treatment of the coupled-wave theory for volume holographic gratings. © *2009 American Association of Physics Teachers.*

[DOI: 10.1119/1.3133089]

I. INTRODUCTION

Volume holographic gratings are routinely used in optical physics. Holographic data storage and optical information processing systems based on volume gratings are currently under development.[1–5] Other applications include polarization optics,[6–8] beam splitters and combiners,[9,10] narrowband spectral filters for optical communications,[11–13] and intracavity Bragg gratings for various types of lasers.[14–16]

A rigorous analysis of volume holographic gratings involves the coupled-wave theory,[17–20] which is derived from Maxwell's equations. Instructors often do not discuss volume holography in undergraduate optics courses because of the difficulty of communicating coupled-wave theory. In this paper, we show that good approximations to volume holographic diffraction can be derived using the multiple beam interference method, which is familiar to students. The results obtained using the multiple beam interference method agree well with those of the coupled-wave theory for weakly modulated gratings.

Consider a dielectric slab with a finite length L, thickness d, and refractive index n_0. For simplicity, we assume that the slab is immersed in a medium with a matched refractive index n_0. A holographic grating is written by optically inducing refractive index variations in the bulk of the slab. Figure 1 shows the model of a volume grating that is used for our analysis. We restrict our attention to lossless transmission gratings. The z-axis is chosen to be in the plane of incidence and normal to the media boundaries, the x-axis is in the plane of incidence and parallel to the media boundaries, and the y-axis is perpendicular to the plane of incidence.

A simple sinusoidal holographic grating can be expressed in terms of the reference and signal monochromatic plane waves of unit amplitude polarized in the $\hat{y}$-direction (s polarization). These waves are denoted by $R=\exp(-i\boldsymbol{\rho}\cdot\boldsymbol{r})$ and $S=\exp(-i\boldsymbol{\sigma}\cdot\boldsymbol{r})$ (see Fig. 1) and interfere inside the photosensitive material. Here $\boldsymbol{\rho}=\beta(-\hat{x}\sin\theta+\hat{z}\cos\theta)$ and $\boldsymbol{\sigma}=\beta(\hat{x}\sin\theta+\hat{z}\cos\theta)$, where $\beta=2\pi n_0/\lambda$ is the average propagation constant and λ is the wavelength in free space. In this paper, we consider a nonslanted symmetric grating with the angles of incidence of the R and S waves to be θ. The intensity distribution of the interference pattern inside the material is given as

$$I \propto |R+S|^2 = 2[1+\cos(\boldsymbol{K}\cdot\boldsymbol{r})], \tag{1}$$

where

$$\boldsymbol{K} = \boldsymbol{\rho} - \boldsymbol{\sigma} = -\hat{x}2\beta\sin\theta \tag{2}$$

is the grating vector. The angle at which the grating was written is defined as the Bragg angle $\theta=\theta_0$.

When the grating in Fig. 1 is illuminated with the plane wave R in the direction of $\boldsymbol{\rho}$ at the Bragg-matched angle θ_0, the plane wave S in the direction of $\boldsymbol{\sigma}$ is reconstructed (Fig. 2). The spatial pattern of the intensity profile creates a grating in the holographic material by modulating the index of refraction of the material so that $n=n_0+\Delta n$, where n_0 is the average refractive index after exposure. Note that the average refractive index of the grating may be slightly different from that of the uniform slab. However, this difference is small and is not important. The hologram (or holographic grating) is defined to be the spatial modulation of the refractive index of the material

$$\Delta n = n_1\cos(\boldsymbol{K}\cdot\boldsymbol{r}), \tag{3}$$

where n_1 is the amplitude of the index modulation in response to the spatial optical intensity distribution inside the material, and the periodicity of the index modulation

$$\Lambda = 2\pi/K = \lambda/(2n_0\sin\theta_0), \tag{4}$$

also known as the grating wavelength, is the same as the periodicity of the light standing wave pattern. In general, the amplitude of the refractive index modulation n_1 is much smaller than that of n_0. For the weakly modulated gratings that we will consider in this paper, typical values are $n_0=1.5$ and $n_1\sim10^{-4}$.

II. COUPLED-WAVE THEORY

In the coupled-wave theory formalism, the read beam R may be incident on the gratings at the Bragg-mismatched angle $\theta=\theta_0+\Delta\theta$, where $\Delta\theta$ is the angular mismatch. The propagation vectors $\boldsymbol{\rho}$ and $\boldsymbol{\sigma}$ contain information about the propagation constants and the directions of propagation of R and the diffracted beam S. We allow the incident beam to deviate from the Bragg angle but keep the incident wavelength fixed. We will assume in the following that the grating is immersed in a medium with a matched average refractive index n_0 so that refraction at the holographic slab boundaries can be ignored. The reference and signal waves $R=R(z)\exp(-i\boldsymbol{\rho}\cdot\boldsymbol{r})$ and $S=S(z)\exp(-i\boldsymbol{\sigma}\cdot\boldsymbol{r})$ are described by amplitudes $R(z)$ and $S(z)$, which vary along the z-direction. The total electric field in the gratings is the superposition of the two waves $E=R(z)\exp(-i\boldsymbol{\rho}\cdot\boldsymbol{r})+S(z)\exp(-i\boldsymbol{\sigma}\cdot\boldsymbol{r})$.

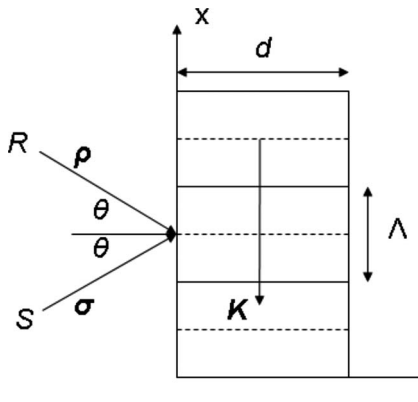

Fig. 1. A simple sinusoidal holographic grating is written by two monochromatic unit amplitude plane waves polarized in the $\hat{y}$-direction (s polarization) $R=\exp(-i\boldsymbol{\rho}\cdot\boldsymbol{r})$ and $S=\exp(-i\boldsymbol{\sigma}\cdot\boldsymbol{r})$ which interfere inside the photosensitive material of thickness d and refractive index n_0. Here $\boldsymbol{\rho}=\beta(-\hat{x}\sin\theta+\hat{z}\cos\theta)$ and $\boldsymbol{\sigma}=\beta(\hat{x}\sin\theta+\hat{z}\cos\theta)$, where $\beta=2\pi n_0/\lambda$ is the average propagation constant, λ is the wavelength in free space, and $\theta=\theta_0$ is the angle of incidence (Bragg angle) in the surrounding medium with a matched average refractive index. The length of the arrow representing the grating vector is obtained from $\boldsymbol{K}=\boldsymbol{\rho}-\boldsymbol{\sigma}=-\hat{x}2\beta\sin\theta$. The periodicity of the grating is $\Lambda=2\pi/K=\lambda/(2n_0\sin\theta_0)$. Solid and dashed horizontal lines represent periodic maxima and minima of refractive index modulation.

We briefly summarize the well-known properties of S as predicted by coupled-wave theory. These properties are for reference and will serve as the benchmarks against which we will compare the prediction of the multiple beam interference model. From Maxwell's equations, we can obtain a system of linear coupled differential equations for R and S, which can be solved subject to the initial conditions $R(0)=1$ and $S(0)=0$.

The diffraction efficiency for symmetric gratings $\eta=|S|^2$ and lossless transmission gratings is defined as

$$\eta_{\mathrm{CWT}}=\frac{\sin^2\sqrt{\nu^2+\xi^2}}{1+\xi^2/\nu^2}=\nu^2\,\mathrm{sinc}^2\left(\sqrt{\nu^2+\xi^2}\right), \tag{5}$$

where $\mathrm{sinc}(x)=\sin(x)/x$. The variables ν and ξ are as defined in Ref. 17, where ν is the grating strength,

$$\nu=\frac{\pi n_1 d}{\lambda\cos\theta_0}, \tag{6}$$

and

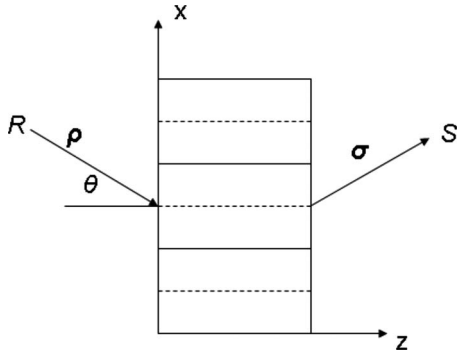

Fig. 2. When the grating in Fig. 1 is illuminated by the plane wave R in the direction of $\boldsymbol{\rho}$ at the Bragg angle $\theta=\theta_0$, the plane wave S in the direction of $\boldsymbol{\sigma}$ is reconstructed.

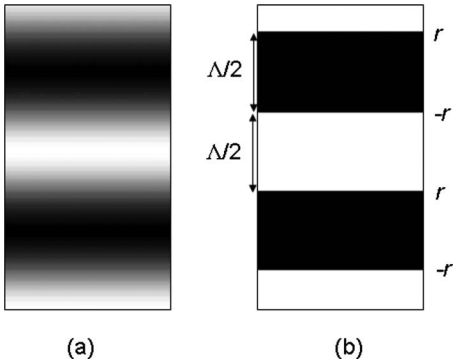

Fig. 3. (a) Sinusoidal refractive index modulation $n(x)=n_0+n_1\cos(2\pi x/\Lambda)$. (b) Equivalent square wave representation $n(x)=n_0+n_1\,\mathrm{sgn}(\cos(2\pi x/\Lambda))$. The reflection coefficients are r at the n_+/n_- interface and $-r$ at the n_-/n_+ interface, where $n_+=n_0+n_1$ and $n_-=n_0-n_1$.

$$\xi=\Delta\theta\frac{\pi d}{\Lambda} \tag{7}$$

is related to the angular deviation from the Bragg angle $\Delta\theta$. For weakly modulated gratings ν ($\nu\ll\xi$),

$$\eta_{\mathrm{CWT}}\approx\nu^2\,\mathrm{sinc}^2(\xi). \tag{8}$$

Diffraction efficiency is a maximum at the Bragg incidence and decays as a sinc^2 function as a result of angular deviation of the read beam from the Bragg condition. Maximum diffraction efficiency for weak modulation (small grating strength) can be estimated as

$$\eta_{\mathrm{CWT}}(0)\approx\nu^2. \tag{9}$$

The full width at half maximum angular bandwidth of the diffraction efficiency can be obtained from the fact that the half power points for a $\mathrm{sinc}^2(\xi)$ function are reached near the values of $\xi\approx\pi/2$. Therefore,

$$\Delta\theta_{\mathrm{FWHM}}=2\Delta\theta_{1/2}\approx\frac{\Lambda}{d}. \tag{10}$$

III. MULTIPLE BEAM INTERFERENCE MODEL

To understand the diffraction from a volume grating, it is useful to visualize the process with the multiple beam interference method. Instead of a sinusoidally varying refractive index model, the grating in this model is visualized as a square wave refractive index modulation with the period Λ

$$n(x)=n_0+n_1\,\mathrm{sgn}(\cos(2\pi x/\Lambda)), \tag{11}$$

where sgn represents the sign function [see Figs. 3(a) and 3(b)]. Here, the grating consists of alternating dielectric layers with refractive indices $n_+=n_0+n_1$ and $n_-=n_0-n_1$. The interfaces between the dielectric layers can be thought of as grating planes separated by a distance $\Lambda/2$. There are a total of $2N$ grating planes, where, for negligible refraction,

$$N=[\text{largest integer}\leq(d\tan\theta/\Lambda)], \tag{12}$$

where θ is the angle of incidence, as shown in Fig. 4. A typical thickness d may vary between 100 μm for photorefractive polymers to 1–10 mm for photorefractive crystals or photopolymers. For an optical wavelength $\Lambda\sim1$ μm so that

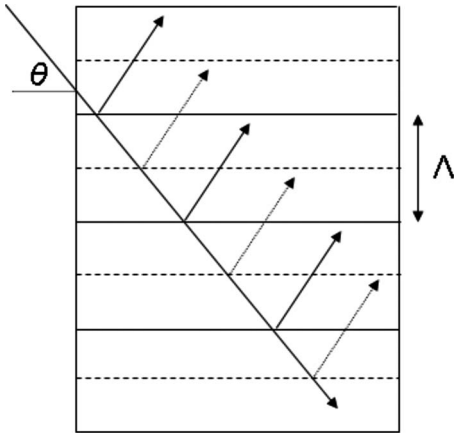

Fig. 4. Multiple beams reflecting from interfaces in the single scattering approximation. Beams reflected from the interfaces with the $+r$ reflection coefficient are shown with solid arrows, and the beams reflected from the interfaces with $-r$ reflection coefficient are shown with dashed arrows. The total number of reflections is $2N$, where for negligible refraction N =[largest integer$\leq(d\tan\theta/\Lambda)$], where θ is the angle of incidence.

a typical value of N is in the range from 100 to 10 000.

The grating planes are characterized by the amplitude Fresnel reflection coefficients r_+ at the n_+/n_- interface and r_- at the n_-/n_+. An incoming beam partially reflects from each of the grating planes it encounters as it traverses the medium. For a wave incident at an angle θ, the reflection coefficient r_+ for s polarization (as considered in this paper) is

$$r_+ = \frac{n_+\cos\theta - n_-\sqrt{1-\left(\frac{n_+}{n_-}\sin\theta\right)^2}}{n_+\cos\theta + n_-\sqrt{1-\left(\frac{n_+}{n_-}\sin\theta\right)^2}}. \tag{13}$$

If we expand in the small argument n_1 and keep only the first-order terms, we obtain

$$\frac{n_+}{n_-} = \frac{n_0+n_1}{n_0-n_1} \approx \left(1+\frac{n_1}{n_0}\right)^2 \tag{14}$$

and

$$\begin{aligned}&\sqrt{1-\left(1+\frac{n_1}{n_0}\right)^4\sin^2\theta}\\ &\quad\approx \sqrt{1-\left(1+4\frac{n_1}{n_0}\right)\sin^2\theta} = \sqrt{\cos^2\theta - 4\frac{n_1}{n_0}\sin^2\theta}\\ &\quad= \cos\theta\sqrt{1-4\frac{n_1}{n_0}\tan^2\theta} \approx \cos\theta\left(1-2\frac{n_1}{n_0}\tan^2\theta\right),\end{aligned} \tag{15}$$

where we have assumed that $0<\theta<\pi/2$. A realistic assumption is to narrow the range of angles of incidence further down to $0<\theta<\pi/3$, for example. Therefore, the numerator in Eq. (13) is

$$\begin{aligned}&(n_0+n_1)\cos\theta - (n_0-n_1)\cos\theta\left(1-2\frac{n_1}{n_0}\tan^2\theta\right)\\ &\quad= 2n_1\cos\theta + \frac{2(n_0-n_1)n_1}{n_0}\cos\theta\tan^2\theta\\ &\quad\approx 2n_1\cos\theta(1+\tan^2\theta) = \frac{2n_1}{\cos\theta},\end{aligned} \tag{16}$$

and the denominator in Eq. (13) is

$$\begin{aligned}&(n_0+n_1)\cos\theta + (n_0-n_1)\cos\theta\left(1-2\frac{n_1}{n_0}\tan^2\theta\right)\\ &\quad= 2n_0\cos\theta - 2\frac{(n_0-n_1)n_1}{n_0}\cos\theta t\tan^2\theta\\ &\quad\approx 2\cos\theta(n_0-n_1\tan^2\theta).\end{aligned} \tag{17}$$

Hence

$$r_+ = \frac{n_1}{\cos^2\theta(n_0-n_1\tan^2\theta)} \approx \frac{n_1}{n_0\cos^2\theta} = r. \tag{18}$$

Similarly,

$$\begin{aligned}r_- &= \frac{n_-\cos\theta - n_+\sqrt{1-\left(\frac{n_-}{n_+}\sin\theta\right)^2}}{n_-\cos\theta + n_+\sqrt{1-\left(\frac{n_-}{n_+}\sin\theta\right)^2}}\\ &\approx -\frac{n_1}{n_0\cos^2\theta} = -r_+ = -r.\end{aligned} \tag{19}$$

Thus we can model the gratings as alternating layers with reflection coefficients r and $-r$ spaced by a distance $\Lambda/2$. For $n_0=1.5$ and $n_1\approx 10^{-4}$, $r\approx 10^{-4}$.

We can derive the analytical expression for the diffraction efficiency by summing reflections from all the grating planes. We assume a single reflection event from each grating plane. The reflections are illustrated in Fig. 4. For the incident unit amplitude electric field, the amplitude of the reflection from each diffraction plane is either $\pm r$. The diffracted electric field is given by a finite sum with alternating sign reflection coefficients. We use the principle of superposition, consider reflections from the interfaces with $+r$ (solid arrows) and $-r$ (dashed arrows) coefficients separately, and then add the two sums together, taking the appropriate phase differences into account. The phase difference between waves reflected by any two successive planes separated by a distance $\Lambda/2$ (that is, reflections with the same sign of the reflection coefficient) is

$$\phi = \beta L, \tag{20}$$

where L is the path length difference. Two reflected rays p_1 and p_2 are shown in Fig. 5. The wave front of the reflected wave is indicated by the dashed line AC. Therefore, the path length difference between the reflections is

$$L = \mathrm{AB} + \mathrm{BC}, \tag{21}$$

where

$$\mathrm{AB} = \Lambda/\sin\theta \tag{22}$$

and

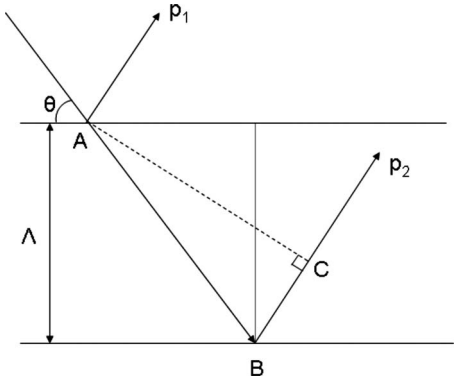

Fig. 5. The phase difference for reflections p_1 and p_2 from two grating planes separated by a distance Λ, that is, with the same reflection coefficients, is $\phi=\beta L$, where the path length difference is $L=\mathrm{AB}+\mathrm{BC}$. For Bragg-matched incidence $\phi_0=2\pi$.

$$\mathrm{BC}=[\Lambda/\sin\,\theta]\cos(\pi-2\theta). \tag{23}$$

Therefore,

$$L=[\Lambda/\sin\,\theta][1-\cos(2\theta)]=2\Lambda\,\sin\,\theta. \tag{24}$$

Hence, the phase difference between the wave fronts reflected by two successive grating planes at Bragg-matched incidence is

$$\phi_0=\beta L_0=2\beta\Lambda\,\sin\,\theta_0=2\frac{2\pi n_0}{\lambda}\frac{\lambda}{2n_0\,\sin\,\theta_0}\sin\,\theta_0=2\pi. \tag{25}$$

For a Bragg-mismatched angle of incidence $\theta=\theta_0+\Delta\theta$, the phase difference is $\phi=\phi_0+\Delta\phi$, where

$$\phi=\beta L=2\beta\Lambda\,\sin\,\theta=\frac{2\pi}{\sin\,\theta_0}\sin(\theta_0+\Delta\theta)$$
$$=2\pi+\Delta\theta 2\pi\cot\,\theta_0, \tag{26}$$

so that

$$\Delta\phi=\Delta\theta 2\pi\cot\,\theta_0. \tag{27}$$

By summing the reflections with coefficient r, we obtain the scalar electric field

$$E_1=r[1+e^{i\phi}+e^{i2\phi}+\cdots+e^{i(N-1)}]=r\frac{1-e^{iN\phi}}{1-e^{i\phi}}$$
$$=re^{i(N-1)\phi/2}\frac{\sin(N\phi/2)}{\sin(\phi/2)}. \tag{28}$$

The waves reflected from the interfaces with reflection coefficient $-r$ have a phase delay $\phi/2$ relative to the waves reflected from the interfaces with $+r$ reflection. Thus we obtain

$$E_2=-re^{i\phi/2}E_1, \tag{29}$$

so that

$$E=E_1+E_2=-r2ie^{i(2N-1)\phi/4}\frac{\sin(N\phi/2)}{\sin(\phi/2)}\sin(\phi/4). \tag{30}$$

Because $\phi=\phi_0+\Delta\phi=2\pi+\Delta\phi$, where $\Delta\phi\ll 1$ is a phase mismatch due to deviation from the Bragg angle, we have

$$|E|=2r\frac{\sin(N\Delta\phi/2)}{\sin(\Delta\phi/2)}\cos(\Delta\phi/4)=r\frac{\sin(N\Delta\phi/2)}{\sin(\Delta\phi/4)}$$
$$\approx r\frac{\sin(N\Delta\phi/2)}{\Delta\phi/4}=2rN\,\mathrm{sinc}(N\Delta\phi/2). \tag{31}$$

Note that $\sin(\Delta\phi/4)$ can be expanded in powers of $\Delta\phi$ but not $\sin(N\Delta\phi/2)$. If we use the values of N in Eq. (12), r in Eq. (18), and $\Delta\phi$ in Eq. (27), we obtain

$$N\Delta\phi/2=\frac{d\,\tan\,\theta_0}{\Lambda}\Delta\theta\frac{2\pi\cot\,\theta_0}{2}=\Delta\theta\frac{\pi d}{\Lambda}=\xi, \tag{32}$$

where ξ was defined in Eq. (7),

$$2rN=2\frac{n_1}{n_0\cos^2\,\theta_0}\frac{d\,\tan\,\theta_0}{\Lambda}=\frac{4\,\tan^2\,\theta_0}{\pi}\frac{\pi n_1 d}{\lambda\,\cos\,\theta_0}=\alpha\nu, \tag{33}$$

$\alpha=4\,\tan^2\,\theta_0/\pi$, and ν was defined in Eq. (6).

Therefore, the diffraction efficiency for the incident wave with unit amplitude is

$$\eta_{\mathrm{MBI}}=|E|^2=(2Nr)^2\,\mathrm{sinc}^2(N\Delta\phi/2)=\alpha^2\nu^2\,\mathrm{sinc}^2(\xi), \tag{34}$$

where we have recovered the $\mathrm{sinc}^2(\xi)$ functional dependence of the diffraction efficiency on the dephasing of coupled-wave theory in Eq. (8). The maximum diffraction efficiency for Bragg-matched incidence for $\Delta\phi=0$ is

$$\eta_{\mathrm{MBI}}(0)=\alpha^2\nu^2. \tag{35}$$

For angles of incidence in the range of $20°\leq\theta\leq 60°$, which is typical for most experimental setups, $0.2<\alpha^2<5$. For $35°\leq\theta\leq 45°$, $\alpha^2\approx 1$. Thus, the maximum diffraction efficiency obtained from coupled-wave theory and the multiple beam interference model agrees within an order of magnitude. The angular full width at half maximum of the diffraction efficiency is the same as for the coupled-wave theory in Eq. (10), $\Delta\theta_{\mathrm{FWHM}}\approx\Lambda/d$.

The functional dependence of observables such as angular bandwidth and diffraction efficiency can be understood transparently from our model. In some cases, such as for angular bandwidth, the agreement is quite good because this quantity is an insensitive function of the index modulation. In other cases, such as for the diffraction efficiency, the agreement is less satisfactory. For example, the diffraction efficiency of the multiple beam interference model in Eq. (35) differs from the coupled-wave theory model by a factor of α^2. In all cases we obtain the proper functional dependence. The multiple beam interference model makes use of a rectangular index modulation profile. In contrast, the coupled-wave theory model is developed for a sinusoidal index variation profile. Thus, the agreement would be more accurate if the coupled-wave theory included the higher order harmonics due to the rectangular nature of the index profile.

To elucidate the dependence of the diffraction efficiency on angular deviation from the Bragg angle, we can formulate the multiple beam interference model with the help of phasors.[21] We represent the reflections from the mth layer in the grating by the phasor

$$p_m=re^{i\phi_m}=re^{im\Delta\phi} \tag{36}$$

for reflections with $+r$ coefficient in Eq. (28) and

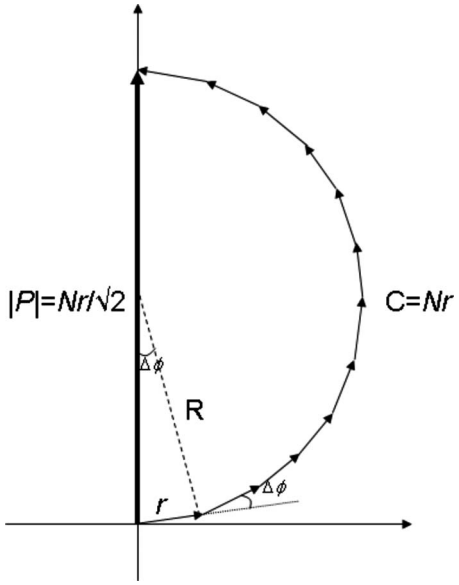

Fig. 6. Phasor diagram illustrating the criteria for half-maximum diffraction dephasing, which occurs when the net phasor with amplitude $|P|=Nr/\sqrt{2}$ coincides with the diameter of the semicircle with radius R formed by the chord of length $C=Nr$.

$$q_m = -re^{i\phi/2}e^{i\phi_m} = re^{i\Delta\phi/2}e^{im\Delta\phi} = e^{i\Delta\phi/2}p_m \tag{37}$$

for reflections with $-r$ coefficient in Eq. (29), where, consistent with Eq. (26)

$$\phi_m = \phi_0 + m\Delta\phi = 2\pi + m\Delta\phi. \tag{38}$$

The sum of the N phasor p_m and N phasor q_m [see Eq. (12)] gives the net phasors

$$P = \sum_{m=0}^{N-1} p_m = r\sum_{m=0}^{N-1} e^{im\Delta\phi} \tag{39}$$

and

$$Q = \sum_{m=0}^{N-1} q_m = e^{i\Delta\phi/2}P. \tag{40}$$

The total electric field phasor is

$$E = P + Q = P + e^{i\Delta\phi/2}P \approx 2P \tag{41}$$

because $\Delta\phi \ll 1$. Note that the zero in diffraction when P and Q have opposite directions, which occurs when $\Delta\phi=2\pi$, can be ignored because it is outside of the region of small $\Delta\phi$. For Bragg-matched diffraction, $\Delta\phi=0$, so that P and Q are collinear and have maximum amplitudes $|P|_{\max}=|Q|_{\max}=Nr$, yielding the maximum diffraction

$$|E|^2_{\max} = (2Nr)^2. \tag{42}$$

When the reading beam deviates from the Bragg angle, $\Delta\phi \neq 0$. For $N \gg 1$ and $r \ll 1$, the vector sum of the reflection phasors forms a curved chord of length $C=Nr$, as illustrated in Fig. 6. Hence the length of the net phasor P decreases. The half-maxima point $\Delta\phi_{\mathrm{HM}}$ of diffraction can be estimated graphically from Fig. 6. Because $|E|_{\mathrm{HM}}=\sqrt{2}Nr$, it follows that $|P|_{\mathrm{HM}}=Nr/\sqrt{2}$. Thus the condition for $\Delta\phi_{\mathrm{HM}}$ is that

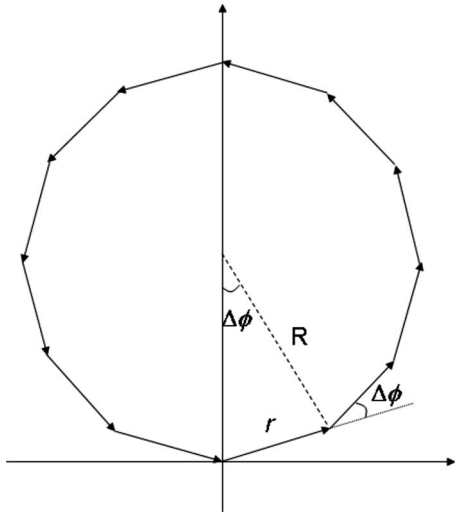

Fig. 7. Phasor diagram illustrating formation of the first zero in diffraction. This zero occurs when the phasors p_m traverse a complete circle with radius R.

$$|P|_{\mathrm{HM}}/C = 1/\sqrt{2}, \tag{43}$$

which occurs when the net phasor P_{HM} coincides with the diameter of the semicircle formed by the chord C because the ratio of the diameter to half circumference is $2/\pi \approx 1/\sqrt{2}$. Therefore, we have $N\Delta\phi_{\mathrm{HM}} \approx \pi$, or

$$\Delta\phi_{\mathrm{HM}} \approx \pi/N. \tag{44}$$

For the value $\Delta\phi_{\mathrm{null}}$ the phasor p_m traverses a complete circle with radius R, as shown in Fig. 7. For $N \gg 1$ and $\Delta\phi \ll 1$, we have the condition of the first zero, that is, $P=0$, and hence, $E=0$ when $N\Delta\phi_{\mathrm{null}}=2\pi$, or

$$\Delta\phi_{\mathrm{null}} = 2\pi/N. \tag{45}$$

As $\Delta\phi$ increases further, the first side lobe begins to appear. Note that the results in Eqs. (42), (44), and (45) are consistent with $|E|^2=(2Nr)^2\,\mathrm{sinc}^2(N\Delta\phi/2)$ in Eq. (34). The advantage of using the phasor description is that it provides an accessible pictorial description of diffraction.

IV. CONCLUSION

In conclusion, we have developed a multiple beam interference model for the interpretation of Bragg diffraction in weakly modulated volume holographic gratings. The multiple beam interference method predicts the same angular diffraction efficiency bandwidth as the coupled-wave theory and is physically intuitive and useful for teaching volume holographic gratings without using coupled-wave theory.

[a]Present address: Nuclear Engineering Division, Argonne National Laboratory, Argonne, Illinois 60439.

[1] A. Heifetz, G. S. Pati, J. T. Shen, J. K. Lee, M. S. Shahriar, C. Phan, and M. Yamamoto, "Shift-invariant real-time edge-enhanced VanderLugt correlator using video-rate compatible photorefractive polymer," Appl. Opt. **45**, 6148–6153 (2006).

[2] A. Heifetz, J. T. Shen, J. K. Lee, R. Tripathi, and M. S. Shahriar, "Translation-invariant object recognition system using an optical correlator and a super-parallel holographic RAM," Opt. Eng. (Bellingham) **45**, 025201 (2006).

[3] L. Hesselink, S. S. Orlov, and M. C. Bashaw, "Holographic data storage systems," Proc. IEEE **92**, 1231–1280 (2004).

[4] M. S. Shahriar, R. Tripathi, M. Huq, and J. T. Shen, "Shared-hardware alternating operation of a super-parallel holographic optical correlator and a super-parallel holographic random access memory," Opt. Eng. (Bellingham) **43**, 1856–1861 (2004).
[5] M. S. Shahriar, R. Tripathi, M. Kleinschmit, J. Donoghue, W. Weathers, M. Huq, and J. T. Shen, "Superparallel holographic correlator for ultrafast database searches," Opt. Lett. **28**, 525–527 (2003).
[6] S. Habraken, Y. Renotte, St. Roose, E. Stijns, and Y. Lion, "Design for polarizing holographic optical elements," Appl. Opt. **34**, 3595–3602 (1995).
[7] J. K. Lee, J. T. Shen, A. Heifetz, R. Tripathi, and M. S. Shahriar, "Demonstration of a thick holographic Stokesmeter," Opt. Commun. **259**, 484–487 (2006).
[8] N. Nieuborg, K. Panajotov, A. Goulet, I. Veretennicoff, and H. Thienpont, "Data transparent reconfigurable optical interconnections based on polarization-switching VCSEL's and polarization-selective diffractive optical elements," IEEE Photonics Technol. Lett. **10**, 973–975 (1998).
[9] H. N. Yum, P. R. Hemmer, A. Heifetz, J. T. Shen, J. K. Lee, R. Tripathi, and M. S. Shahriar, "Demonstration of a multiwave coherent holographic beam combiner in a polymeric substrate," Opt. Lett. **30**, 3012–3014 (2005).
[10] M. S. Shahriar, J. Riccobono, M. Kleinschmit, and J. T. Shen, "Coherent and incoherent beam combination using thick holographic substrates," Opt. Commun. **220**, 75–83 (2003).
[11] S. Datta, S. R. Forrest, B. Volodin, and V. S. Ban, "Low through channel loss wavelength multiplexer using multiple transmission volume Bragg gratings," J. Opt. Soc. Am. A Opt. Image Sci. Vis. **22**, 1624–1629 (2005).
[12] D. D. Do, N. Kim, T. Y. Han, J. W. An, and K. Y. Lee, "Design of cascaded volume holographic gratings to increase the number of channels for an optical demultiplexer," Appl. Opt. **45**, 8714–8721 (2006).
[13] D. Iazikov, C. M. Greiner, and T. W. Mossberg, "Integrated holographic filters for flat passband optical multiplexers," Opt. Express **14**, 3497–3502 (2006).
[14] G. Ewald, K. M. Knaak, S. Gotte, K. D. A. Wendt, and H. J. Kluge, "Development of narrow linewidth diode lasers by use of volume holographic transmission gratings," Appl. Phys. B: Lasers Opt. **80**, 483–487 (2005).
[15] B. L. Volodin, S. V. Dolgy, E. D. Melnik, E. Downs, J. Shaw, and V. S. Ban, "Wavelength stabilization and spectrum narrowing of high-power multimode laser diodes and arrays by use of volume Bragg gratings," Opt. Lett. **29**, 1891–1893 (2004).
[16] Y. J. Zheng and H. F. Kan, "Effective bandwidth reduction for a high-power laser diode array by an external cavity technique," Opt. Lett. **30**, 2424–2426 (2005).
[17] H. Kogelnik, "Coupled wave theory for thick hologram gratings," Bell Syst. Tech. J. **48**, 2909–2947 (1969); reprinted in *Selected Papers in Fundamental Techniques in Holography*, edited by H. I. Bjelkhagen and H. J. Caulfield (SPIE, Bellingham, WA, 2001), pp. 44–82.
[18] M. G. Moharam and T. K. Gaylord, "Rigorous coupled-wave analysis of planar-grating diffraction," J. Opt. Soc. Am. **71**, 811–818 (1981).
[19] K.-Y. Tu, T. Tamir, and H. Lee, "Multiple-scattering theory of wave diffraction by superimposed volume gratings," J. Opt. Soc. Am. A **7**, 1421–1435 (1990).
[20] A. Heifetz, J. T. Shen, S. C. Tseng, G. S. Pati, J. K. Lee, and M. S. Shahriar, "Angular directivity of diffracted wave in Bragg-mismatched readout of volume holographic gratings," Opt. Commun. **280**, 311–316 (2007).
[21] F. A. Jenkins and H. E. White, *Fundamentals of Optics*, 4th ed. (McGraw Hill, New York, 1976).

ONLINE COLOR FIGURES AND AUXILIARY MATERIAL

AJP uses author-provided color figures for its online version (figures will still be black and white in the print version). Figure captions and references to the figures in the text must be appropriate for both color and black and white versions. There is no extra cost for online color figures.

In addition AJP utilizes the Electronic Physics Auxiliary Publication Service (EPAPS) maintained by the American Institute of Physics (AIP). This low-cost electronic depository contains material supplemental to papers published through AIP. Appropriate materials include digital multimedia (such as audio, movie, computer animations, 3D figures), computer program listings, additional figures, and large tables of data.

More information on both these options can be found at www.kzoo.edu/ajp/.